

# DYNAMIC ROUGHNESS AS A MEANS OF LEADING EDGE SEPARATION FLOW CONTROL

**P. D. Gall\***, **W. W. Huebsch\*** and **A.P. Rothmayer\*\***

\*West Virginia University, Morgantown, WV

\*\*Iowa State University, Ames, IA

**Keywords:** *dynamic roughness, separation bubble, flow control*

## Abstract

*The aircraft industry, as a whole, has been deeply concerned with improving the aerodynamic efficiency of current and future flight vehicles, particularly in the commercial and military markets. However, of particular interest to the field of aerodynamics is the elusive concept of a workable flow control mechanism. Effective flow control is a concept which if properly applied can increase aerodynamic efficiency. Various concepts and ideas to obtain successful flow control have been studied in an attempt to reap these rewards. Some examples include boundary layer blowing (steady and periodic), suction, and synthetic jets. The overall goal of flow control is to increase performance. The specific objectives of flow control include: 1) delay or eliminate flow separation, 2) delay boundary layer transition or 3) reduce skin friction drag. The purpose of this research is to investigate dynamic surface roughness as a novel method of flow control technology for external boundary layer flows. As opposed to standard surface roughness, dynamic roughness incorporates small time dependent perturbations to the surface of the airfoil. These surface perturbations are actual humps and/or ridges that are on the scale of the laminar boundary layer, and oscillate with an unsteady motion. Research has shown that this can provide a means to modify the instantaneous and mean velocity profile near the wall and favorably control the existing state of the boundary layer. The results of this study have shown that dynamic roughness can be a viable alternative in delaying and/or eliminating the leading edge laminar*

*separation bubble and hence reaping some of the rewards of an effective flow control system, while also maintaining some physical advantages over other techniques.*

## 1 Introduction

The aerospace community is continually searching for methods to improve the aerodynamic efficiency of current and future flight vehicles, particularly in the commercial and military markets. Upon reviewing recent emerging technologies, it is apparent that there have been many advancements in several areas of design such as aerodynamics, structures, propulsion, and controls. However, of particular interest to the field of aerodynamics is the elusive concept of a workable flow control mechanism. With respect to separation, this is particularly important for low Reynolds number airfoil ranges where laminar separation bubbles become an ever present phenomenon [1]. Many airfoil applications fall into this range such as mid and high altitude UAV's, sailplanes, jet engine fan blades, inboard helicopter rotor blades, wind turbine rotors, and propellers at high altitudes. Also, there has been recent interest in micro-air vehicles (MAV's) which also fall into this range. To apply flow control means altering the flow field over an airfoil or body in order to improve its efficiency.

Many conceptual solutions to the flow control problem have been proposed, some holding a much greater potential for successful implementation than others [2,3]. There are, however, several reasons why most of these

concepts have not been implemented into mainstream manufacturing. Some systems actually have a higher power usage requirement than power savings, resulting in a net energy loss [4]. Other flow control systems have a very narrow operating envelope for control authority; when flow control is attempted in off-design conditions, the flow control system fails. Also, in some cases the high cost or complexity of the airfoil flow control system is simply not feasible. In other cases the system appears operational in the lab environment, but experiences difficulties when applied in the field. Therefore, designing a mechanism which can overcome these fundamental flaws could prove a significant advancement in improving the aerodynamic efficiency of flight vehicles ranging from micro air vehicles (MAV) to large transport category aircraft. Dynamic roughness may offer distinctive advantages over other proposed systems. Examples are no holes or ports which can be susceptible to clogging. Also, it appears the power requirements for such a system are minimal when compared to blowing or suction.

The global goals of flow control are to increase performance by increasing lift, reducing drag, and improving stall characteristics. The specific objectives of flow control are usually achieved through one of the following: 1) delay or eliminate flow separation, 2) delay boundary layer transition or 3) reduce skin friction drag. From an aerodynamic standpoint, proper flow control mechanisms have the potential to decrease skin friction and form drag, increase lift, improve flight controllability and maneuverability, and provide significant savings in overall fuel consumption. For example, maintaining laminar flow over the entire wing surface can reduce total aircraft drag by as much as 15% [5]. In the commercial aircraft industry, an overall drag reduction of just 1% can translate to millions of dollars saved in annual fuel costs.

The purpose of this research is to investigate dynamic roughness as a novel method of flow

control technology for external boundary layer flows. As apposed to normal surface roughness, dynamic roughness incorporates small time dependent perturbations to the surface of the airfoil. These surface perturbations are actual humps and/or ridges on the surface of the airfoil that are on the scale of the local boundary layer, but with an unsteady motion. When dynamic roughness amplitude is smaller than or comparable to the existing boundary layer height, it has been shown to provide a means to modify the instantaneous and mean velocity profile near the wall and control the local state of the boundary layer, which provided suppression of leading edge flow separation [6,7]. The authors believe that some possible explanations for the flow control are the alteration on flow instabilities, the creation of hairpin type vortices in the viscous sub layers of the boundary layer which enhances mixing and entrainment, the creation of artificial Reynolds stresses, or the favorable alterations of the pressure gradient (or a combination of the above). When dynamic roughness amplitude is on the same order as the height of the boundary layer, it tends to completely alter the state of the boundary layer. For example, when a laminar boundary layer is approaching the leading edge of an airfoil under certain conditions of Reynolds number and angle of attack, a separation bubble will normally form. When dynamic roughness is sized on the scale of the approaching boundary layer and introduced just upstream of the separation point, then the state of the approaching boundary layer will be altered prior to it reaching the natural separation point [6,7]. This altered state is completely different from the laminar boundary layer which originally tended towards separation. This was evident in the results of the experimental study. This new artificial state has different separation, stability, and transition properties, and is expected to produce surface forces that are significant enough to alter the lift and drag of the airfoil. This study has shown that dynamic roughness, if correctly applied, can suppress separation and increase the efficiency of a given airfoil.

## **2 Conceptual Basis**

Using a two-dimensional Navier-Stokes solver, Huebsch [6,7] showed that the leading edge separation bubble could be entirely eliminated and the downstream vortex shedding created by the separation bubble could be minimized. A similar result may be seen in Figure 5, though not showing the details of the flow within the boundary layer which can be found in Huebsch [6,7]. Figure 5a and the work of Huebsch shows that the flow about the leading edge changes to an attached flow when the dynamic roughness is turned on, without any significant large scale unsteadiness in the flow. In fact, the work of Huebsch [6,7] shows that the only unsteadiness in the flow is a small scale unsteady separation located right at the dynamic roughness elements. There is no evidence of large scale unsteady separation, significant flow instabilities or transition elsewhere in the flow. This means that the small scale unsteady surface roughness is completely altering the state of the flow along the entire leading edge. The leading edge becomes attached and laminar when the dynamic roughness is turned on, whereas it is highly separated with significant unsteadiness when the dynamic roughness is turned off (see Figs. 8 and 9). As noted above, this result is perhaps to be expected. Dynamic roughness which takes up a significant fraction of the boundary will completely alter the local state of the boundary layer over the entire region where the dynamic roughness is located. In effect, the dynamic roughness is creating its own local flow field which, in principle, will induce Reynolds stresses within the boundary layer. The authors believe that it is possible that these Reynolds stresses are acting in such a way as to accelerate the boundary, thereby avoiding separation. It should be noted that other unsteady three-dimensional effects, such as the creation of hairpin eddies about the dynamic roughness, could also act to energize the boundary layer. While the study of Huebsch [6,7] concentrated on dynamic roughness elements whose sizes were comparable to the boundary layer thickness, and which could clearly disrupt the boundary

layer, the current study shows that this global alteration of the boundary layer can be maintained even when the amplitude of the dynamic roughness decreases to a few percent of the boundary layer thickness (see Fig. 7), providing that the frequency is significantly increased. This result makes sense from a Reynolds stress perspective. The Reynolds stresses within the boundary layer are created by the flow velocities which are generated by the velocity of the moving roughness elements. If the amplitude of oscillation is decreased but the frequency is increased then the velocity magnitudes within the boundary layer induced by the dynamic roughness can be maintained, and the effective magnitude of the Reynolds stresses induced by the dynamic roughness can also be maintained. These ideas are currently being explored in a more rigorous setting.

## **3 Numerical Analysis**

The initial phase of this study focused on simulating a two-dimensional case (similar to the previous work of Huebsch [6]) in the commercial code Fluent to validate the code with experimental data. The code utilizes a finite volume Navier-Stokes implicit type solver [9]. Several user defined function algorithms (UDF's) were developed that simulated the motion of the dynamic roughness. Acceptable grid remeshing proved to be a tedious process. A combination of several parameters in the layering, smoothing and remeshing algorithms required extensive tailoring in order to obtain a mesh which would properly readapt to the moving dynamic roughness. Results of the two-dimensional study were comparable to the results found in reference [6]. The next step was to develop a fully functional three-dimensional model, also with Fluent, which would simulate the flow past three-dimensional roughness.

For the three-dimensional model a C-type grid was constructed. The grid extends three chord lengths upstream, four chord lengths downstream and four chord lengths above and

below the wing. Although it is common for the far field region of many grids to extend beyond these ranges, these values were chosen to be adequate since the emphasis of this research is the boundary layer flow physics near the surface. Once the domain was established, an unstructured mesh was carefully constructed using a combination of tetrahedral and triangular type cells in a manner which would allow good resolution of the flow physics while at the same time managing the overall cell count. When applying moving walls, it is a requirement of the code that the mesh consist of tetrahedron type cells in order for the remeshing algorithms to function correctly. Specific zones on the surface of the airfoil were identified and constructed which would each represent a compliant type surface in which the motion would be governed by its corresponding user defined function (UDF). The basic airfoil was modeled to have a one meter chord length and a thickness ratio of 12% (NACA 0012). The dynamic roughness initially consisted of a series of 14 humps placed in 14 zones beginning at the 0.6% chord location and extending to the 3.2% chord location. The first location was chosen based on the fact that the normal separation point for this airfoil application is downstream of the 1% chord location. This would allow the roughness field to be located just upstream of the normal laminar separation point. The chordwise length of each zone was 2 mm (0.2% chord) which corresponds to the wavelength of each individual roughness element. The hump geometry was initially shaped like a rotated axisymmetric sine wave function and had a maximum amplitude of 1 mm (0.1% chord) and a total wavelength of 2 mm (0.2% chord). The frequency and amplitude of each individual row of humps could be changed by adjusting parameters in the UDF. These initial analysis values were chosen based on previous research which indicated that the roughness height is most effective when its amplitude is approximately 50-80% of the oncoming boundary layer height. [6,7]. The boundary layer in the region of the first hump is approximately 1.4 mm (0.14% chord) in thickness. Figure 1 depicts a portion of the three-dimensional grid.

After defining the compliant wall zones, the mesh had to be carefully created. A fine resolution was required in the hump region in order to capture the small scale flow physics. Therefore, in the region of the dynamic roughness, the grid spacing was approximately 20 nodes in the chordwise direction over each hump. This same spacing was used in the spanwise direction for the three-dimensional model. Successive grid spacing was held to a maximum growth factor of 1.2. Figure 2 is a shaded view of two of the types of surfaces that were studied. One case represents axisymmetric three-dimensional humps and the other case represents spanwise ridges. The spanwise ridges taper in a sinusoidal fashion to flush with the airfoil surface near the tip of the span. Analysis of results focused on the central region of the span.

In this study a laminar flow analysis was used. The reasons for this are as follows: 1) the separation bubble is a laminar flow phenomenon; if the flow were to be all turbulent the separation bubble would not form for these flow conditions 2) the leading edge region of most airfoils is primarily a laminar flow region and 3) if we continue to increase the resolution of the flow domain in this region, we eventually reach a point where the flow approaches the threshold of DNS modeling, depending on the Reynolds number and smallest turbulence length scale, which inherently requires no turbulence modeling. Therefore, this flow type was selected and used throughout the entire flow domain except for the examination of some special cases.

#### 4 Results of Numerical Analysis

It has long been understood that surface pressure, and the corresponding pressure gradient is one of the dominant factors in determining the behavior of the separation bubble. Therefore, the effects that dynamic roughness have on the pressure distributions in the leading edge region will be examined first. For the clean airfoil the basic pressure distribution is quite predictable and corresponds well with experimental data. The NACA 0012

airfoil, being an airfoil that is not designed for extensive laminar flow, has a pressure distribution curve that quickly peaks close to the leading edge where maximum suction pressure and maximum velocity are reached. This results in a smooth and rather gradual pressure recovery. This can be observed in figure 3 which focuses on the pressure coefficient on the upper surface very close to the leading edge. The pressure distribution for the dynamic roughness represents a temporal snapshot of the humps when they are at their maximum amplitude during the expansion-contraction cycle. This case was run at 12 degrees angle of attack and a Reynolds number of 100,000. Figure 4 depicts a snapshot of the pressure distribution over the humps at four different positions in the cycle. The intent is to show how the pressure varies as a function of hump position. It can also be observed that although the overall magnitude of the pressure coefficient changes, the slope of the pressure coefficient curve does not vary significantly. It is unclear how sensitive the boundary layer may be to very small changes in the pressure gradient. As previously discussed, it appears that the effect of the dynamic roughness is to alter the flow physics in such a fashion that the boundary layer separation may be delayed and/or eliminated entirely. This combined with the resulting pressure distributions tend to produce favorable global effects on the lift and drag coefficients.

Figure 5 shows a display of two wing sections, one with dynamic roughness and the second a smooth surface. The favorable effects of the dynamic roughness can be observed in the pathlines as well as the surface pressure coefficient. From figure 5, the first clear observation is that in the clean case, the flow immediately separates. The flow remains separated creating a large separation bubble. In the case of dynamic roughness, the flow remains attached throughout the roughness field and remains attached further downstream. Eventually the flow separates further downstream when the adverse pressure gradient resulting from the pressure recovery creates instabilities that the boundary layer cannot

overcome. It is critical to realize that these cases were run with no turbulence modeling. Based on experimental results presented below, the authors believe that this downstream separation is an artifact of forced laminar flow and is not physical. A second observation is the three-dimensional surface pressure. When the flow becomes attached to the surface in the field of the dynamic roughness, the improvement in the suction pressure can be observed, as expected. This directly leads to more lift and less drag in the form of favorable “leading edge suction”.

A fundamental part of understanding the benefits of flow control lies in the understanding the changes effective flow control has on the local shear stress distribution. The drag of an airfoil primarily consists of two components, the tangential viscous shearing forces and the normal pressure forces. Immediately downstream of the stagnation point, the shear stress levels are normally quite high due to the early development of the boundary layer and the large values of the velocity gradient near the wall. As the boundary layer develops, the magnitude of the velocity gradient decreases and the shear stress levels decrease. When the boundary layer is turbulent, the velocity gradient is much higher than in the laminar case, and hence the turbulent skin friction drag is much higher.

Figure 6 is a plot of the surface shear stress levels in the leading edge region of the airfoil at 12 degrees angle of attack and a Reynolds number of 100,000. Included in this figure are wall shear stress results for a clean wing using laminar and turbulent flow simulations and a dynamic roughness wing using the laminar solver. Let us consider the flow over the bubble region. In this region the flow is relatively stagnant near the wall except where a vortex exists close to the surface. For this reason the shear stress levels are quite low. Considering the roughness region, there exists a shear layer over the humps where the flow is close to stagnant near the wall. In the valleys located between the humps the shear stress is low. At the peaks of the humps, where the flow is attached, a rise in the local shear stress levels

can be observed. As this shear layer thickens further downstream, this effect becomes less and less pronounced so that the overall effect is a significant reduction in local shear stress versus the turbulent attached case, which is also shown in figure 6 for comparison purposes. For the clean wings, the turbulent boundary layer is able to suppress the separation bubble, but has a higher wall shear stress than the laminar case. The dynamic roughness wing is also able to suppress the bubble, but has similar wall shear to the clean laminar case. This translates to a drag reduction.

### 5 Amplitude and Frequency Effects on Flow Control

Several parametric studies were carried out in order to begin quantifying the effects of amplitude and frequency on the effectiveness of dynamic roughness. Several cases were run for various frequencies and amplitudes ranging from a very shallow roughness height (1% oncoming boundary layer thickness) to a roughness height equal to about 80% of the boundary layer height and frequencies ranging from 30 Hz to 120 Hz. Numerical results indicated that flow control could be obtained with amplitudes as small as 1% of the oncoming boundary layer height, provided the frequency is high enough. The lack of flow control was characterized by the separation point on the leading edge remaining relatively unchanged compared to the clean case. Effective flow control was characterized when the separation bubble was eliminated. The numerical analysis also indicated a somewhat transient state referred to as a ‘buffer zone’. In these cases, the flow appeared to separate in the roughness region forming a very thin shear layer. However, once passing through the roughness field, the flow then reattached to the airfoil surface. Therefore, this buffer region is a fluctuating state between full control and loss of control. In some cases, at some point beyond the roughness field, the flow would eventually separate. This was believed to be due to the fact that the Navier-Stokes solver was applied with no turbulence modeling. In actual situations, it is believed that the boundary layer, once leaving

the roughness field in a laminarized state, undergoes a natural transition process. The experimental results have qualitatively shown this to be the case. Figure 7 is a summary of the expected flow field as a function of amplitude and frequency from the CFD results. Each data point represents a separate case where the flow field was analyzed. There appears to be a correlation between the amplitudes and frequencies where flow control is effective. For the case of 12 degrees angle of attack and a Reynolds number of 100,000 this occurs at around 60 Hz. These numerical results are also consistent with the experimental work. As the amplitude of the roughness is decreased it appears that a higher frequency is required to obtain flow control. Conversely, a larger amplitude requires lower frequency to maintain control. This seems plausible since generating a certain level of artificial Reynolds stresses at lower amplitudes would require higher frequencies of motion. Also, it is significant to note that the critical roughness Reynolds number is about 100 for the humps at maximum amplitude. The critical roughness Reynolds number normally required for forced transition is about 600. This clearly explains why static roughness at the same maximum hump amplitudes does appear to cause transition.

### 6 Experimental and Numerical Results and Comparison

A NACA 0012 airfoil was tested in the West Virginia University flow visualization wind tunnel. The model had a 151 mm span and a 152 mm chord. It was tested at Reynolds numbers of 100,000 and 150,000. Figure 8 is a depiction of the experimental model. The mechanism used to create the dynamic roughness consisted of a thin latex rubber (0.08 mm thickness) sheet cemented to a thin wire mesh. The actuation was created by pressurizing the roughness apparatus with an oscillating air pressure source. Flow visualization and pressure measurements were used to experimentally study the effectiveness of dynamic roughness. There were five pressure ports installed on the baseline clean airfoil model and two pressure ports installed on the dynamic roughness model

(downstream of the roughness region). The limited number of pressure ports was due to the fact that they were added after the model had been fabricated. Although limited, the pressure was used to confirm the anticipated changes in surface pressures. The first phase of the experiment dealt with testing the clean airfoil in order to study and document the existence of the separation bubble and its characteristics at various Reynolds numbers and angles of attack, then compare this data to previous studies. The second and third phases dealt with studying a short and long separation bubble respectively. These results compared well for this particular airfoil at angles of attack up to 12 degrees.

### **6.1 Short Separation Bubble**

The second phase of this experiment was to evaluate the effects of dynamic roughness on a short separation bubble. Figure 9 displays the airfoil at 9.5 degrees angle of attack. To the left in the figure is the experimental flow visualization and to the right is a close-up of the CFD analysis near the leading edge region. Before the dynamic roughness is actuated, the airfoil behaves as a clean airfoil exhibiting a classic short separation bubble. Figures 9a and 9b represent a short separation bubble separating about the 2% chord location and reattaching at approximately the 25% chord location. Also, in this figure the dynamic roughness apparatus mounted in the airfoil leading edge can be observed. The first roughness element is at about the 3.0% chord location and the aft roughness element is located at about the 10.1% chord location. Although based on previous work [6] it was thought that the first roughness element needed to be upstream of the separation point. In this experiment the location was just aft of the separation point due to model fabrication constraints. As the roughness is actuated, effective flow control begins to take place. In figures 9a and 9b the dynamic roughness has not been actuated. In figures 9c and 9d the frequency has been increased to 60 Hz and it appears that the dynamic roughness flow control mechanism has eliminated the separation bubble. As the frequency is increased further the

flow simply appears to remain attached. This finding is consistent with the numerical analysis. The maximum frequency obtainable in the experiment was 160 Hz. Theoretical studies have been done indicating effective flow control for frequencies ranging up to several thousand Hertz. However, it would be considered desirable to obtain effective flow control at lower frequencies due to simpler implementation.

It is of significance to examine the pressure distribution on the upper surface of the airfoil. Figure 10 is a plot of the pressure distribution on this particular airfoil. The solid line represents data taken from Rinoi and Takemura [8] at a slightly higher Reynolds number of 130,000. Also plotted in the figure is the actual pressure measurements taken in this experiment at a Reynolds number of 100,000. The second set of data points, shown by the green symbols, represents the clean airfoil case where five static pressure ports were located. The third set of data points, shown as red symbols, represents the two pressure measurements taken with the dynamic roughness apparatus in place. Many more pressure orifices would have been desirable, but due to the challenge of adding the ports after model was fabricated, it was only possible to install two. Typically, once a short bubble forms, there is only a small variation in surface pressure. The presence of the short bubble is usually signaled by a slight plateau in the pressure curve. Once the dynamic roughness is actuated and the boundary layer becomes attached, it is not surprising to see only a very slight change in the pressure. It is the intent of this figure to show that although the dynamic roughness suppresses the separation bubble, it does not significantly alter the pressure distribution. It is believed to be, however, a precursor leading to the suppression of the long bubble.

### **6.2 Long Separation Bubble**

The case of the long separation bubble presents the most desirable case for applying effective flow control. When a long separation bubble exists, the pressure distribution can be greatly

altered. Generally, a long separation bubble results in a significant loss of lift at a given angle of attack, i.e. the classic leading edge stall. At 12 degrees angle of attack, a long and highly unsteady separation bubble can be observed. Figures 11a and 11b shows the airfoil at 12 degrees angle of attack prior to actuation of the dynamic roughness. The separation point is clearly observed, however it is unclear at what point the flow reattaches to the airfoil. Figures 11c and 11d also shows the state of the flow after the dynamic roughness has been actuated. The frequency at this instant is 60 hertz. The separated flow has reattached itself to the surface and the dynamic roughness appears to provide effective flow control. However, in the numerical calculation, downstream of the reattachment a secondary separation can be observed. This is believed to be due to the code being run with no turbulence modeling. It is believed that in reality like experiment, the boundary layer, after passing through the dynamic roughness field, undergoes a natural transition process which allows it to remain attached. This was verified by inducing a turbulence model downstream of the roughness and observing the flow. This is a capability of the code and allows the user to set up a zone where a laminar flow may be “seeded” with a turbulence model if one knows the precise location where this may occur. This change in pressure can also be observed in the numerical analysis. The dark blue represents a higher negative pressure coefficient. As the flow control begins to take effect, the region of suction pressure increases. As the frequency is further increased, the flow simply appears to remain attached.

The pressure distribution case for the long bubble is significantly different than the short bubble. For the clean airfoil case, leading edge suction tends to collapse and the pressure recovery becomes very gradual. When the dynamic roughness is actuated, the attached flow alters the pressure distribution. The suction pressure is restored and the distribution approaches that of an attached flow. This, of course, results in a significant increase in lift at a given angle of attack and an increase in

leading edge suction (drag reduction). The intent of figure 12 is to show the changes in pressure when the long separation bubble is suppressed. Although the pressure measurements taken are quite limited, the intent was to successfully demonstrate a recovery of suction pressure. The figure depicts the clean airfoil pressure distribution taken from reference 8 as well as displaying the pressure measurements taken in this experiment. The results of this experimental and numerical study clearly show that dynamic roughness can be an effective means of flow control when leading edge separation is present and is a precursor to a leading edge type stall.

## 7 Conclusions and Recommendations

In this research effort, two-dimensional and three-dimensional simulations were performed in order to evaluate the mechanism of dynamic roughness as a means to provide effective leading edge flow control. In addition, wind tunnel experiments were performed to validate the concept. The model used in this study was a NACA 0012 airfoil at a Reynolds number of 100,000 and 150,000. Numerical analysis was accomplished using the commercial code Fluent. The code was set up to accommodate the unsteady flow physics involved in laminar separations and moving walls (dynamic roughness).

Results of this study indicate that dynamic roughness can be used as an effective means of leading edge flow control. Dynamic roughness has the ability to eliminate both the short and long separation bubbles inherent in a low Reynolds number leading edge flow operating at a moderate angle of attack. Also, roughness amplitudes along the order of only a few percent of the boundary layer thickness can provide flow control, provided the frequency is high enough. In addition, there appears to be a frequency threshold below which the dynamic roughness acts as static roughness and is ineffective. This type of flow control has the potential to be more efficient than the traditional boundary layer control methods. Also, a significant finding was that in the experimental

case, the dynamic roughness field actually originated downstream of the theoretical separation point. This was due to fabrication constraints in building the model. In spite of this, the flow visualization showed that the dynamic roughness still eliminated the separation bubble. This implies that perhaps this method is more robust than previously thought and may adapt well to off design conditions. Given the results of this study, it seems justifiable to continue research in this area. Future work should include:

- Refinement of the numerical methods applied in studying three-dimensional parameter space. These parameter may include roughness height, location, frequency dependence, and geometry.
- Continued experimental studies bases on the numerical results. Experimental studies could include detailed surface pressure measurements along the entire surface, continued flow visualization techniques, and detailed velocity measurements of the flow near the surface of the airfoil.
- Evaluation of mechanisms to provide the dynamic roughness field. Some of these mechanisms include pzieoelectric actuation, liquid crystal actuation, and pure mechanical actuation.

## References

- [1] McCullough G and Gault D. "Examples of representative types of airfoil section stall at low speed," *NACA Technical Note 2502*.
- [2] Greenblatt D and Wagnanski, I. "The control of flow separation by periodic excitation," *Progress in Aerospace Sciences*, pp 487-545, Elsevier Pergamon, 2000.
- [3] Gad-el-Hak M. "Flow control: the future," *AIAA Journal of Aircraft*, Vol. 38, pp402-417, 2001.
- [4] Bushnell D and Hefner J. "Effect of compliant wall motion on turbulent boundary layers", *Physics of Fluids*, Vol. 20, No. 10, pp S31-S48, 1977.
- [5] Schrauf G. "Application of laminar flow technology on transport aircraft," *CEAS Drag Reduction Conference*, 2000.
- [6] Huebsch W. "Two-dimensional simulation of dynamic surface roughness for aerodynamic flow

control," *Journal of Aircraft*, Vol. 43, No. 2, pp 353-362, 2006.

[7] Huebsch, W., "Dynamic surface roughness for aerodynamic flow control," *AIAA-2004-587*, 42<sup>nd</sup> AIAA Aerospace Sciences Meeting and Exhibit, Jan 5-8, Reno, Nevada, 2004.

[8] Rinoie, K and Takemura, N., "Oscillating behavior of laminar separation bubbles Formed on an aerofoil near stall," *The Aeronautical Journal*, pp 153-163, March 2004.

[9] Fluent Inc., "Fluent User's Guide," [Fluent](http://www.fluentusers.com), 2009.

## Copyright Statement

The authors confirm that they, and/or their company or organization, hold copyright on all of the original material included in this paper. The authors also confirm that they have obtained permission, from the copyright holder of any third party material included in this paper, to publish it as part of their paper. The authors confirm that they give permission, or have obtained permission from the copyright holder of this paper, for the publication and distribution of this paper as part of the ICAS2010 proceedings or as individual off-prints from the proceedings.

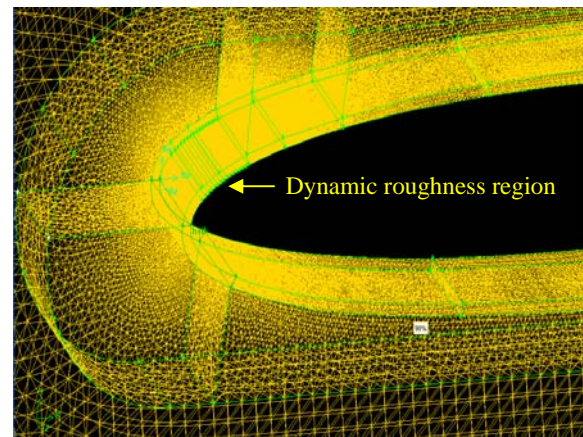
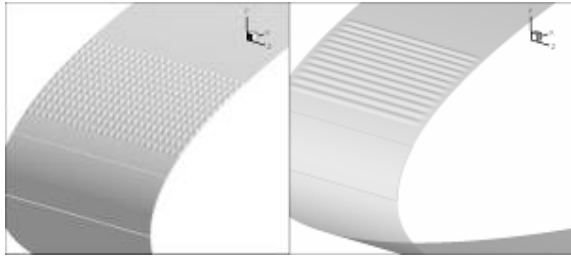


Fig. 1. Three-dimensional mesh



a) Three-dimensional humps b) Two-dimensional ridges

Fig. 2. Dynamic roughness airfoil surfaces with dynamic roughness fully actuated.

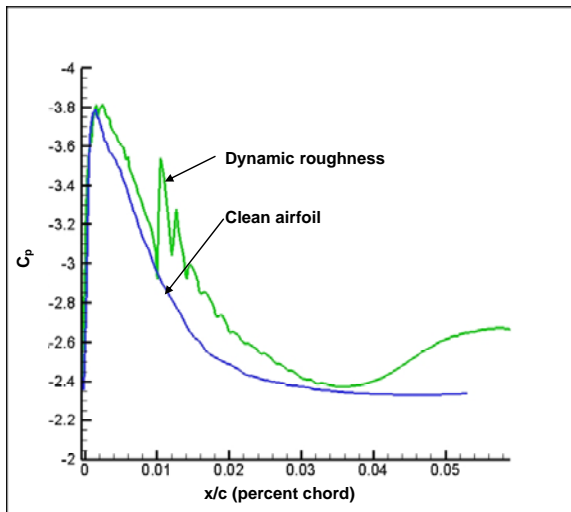


Fig.3. Leading edge pressure distribution.

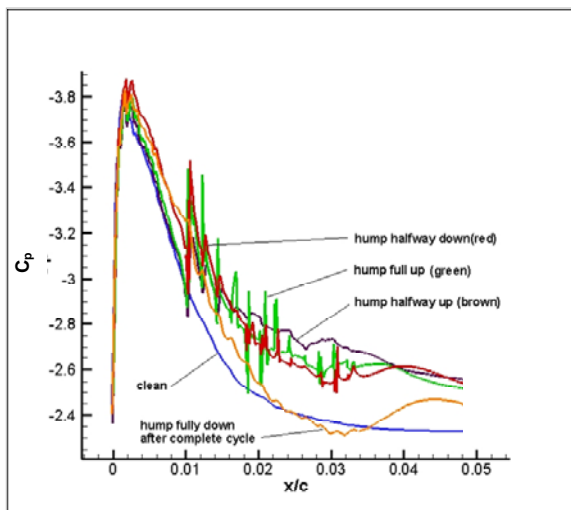


Fig. 4. Pressure distributions for clean and dynamic roughness wings throughout hump cycle in the leading edge region.

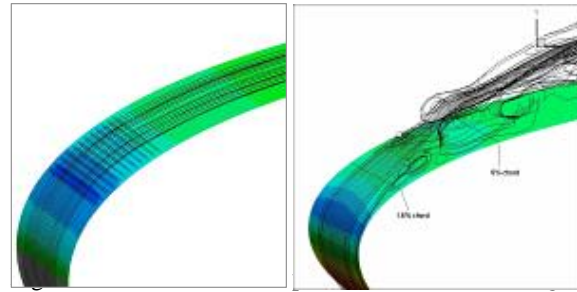


Fig. 5. Contours of surface pressure distribution along with near-wall pathlines for dynamic roughness actuation (left) and clean wing (right).

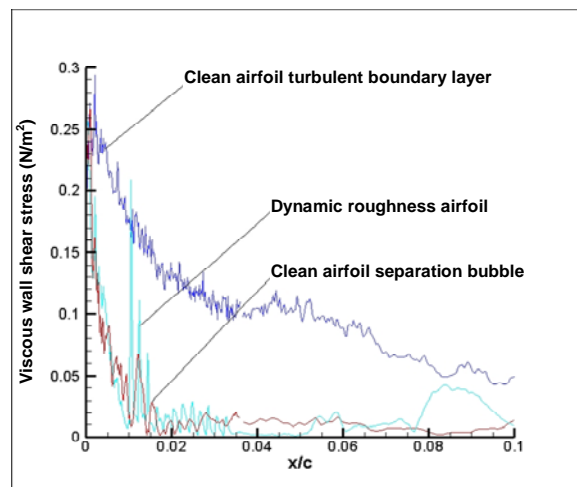


Fig. 6. Wall shear stress values for clean laminar, clean turbulent, and dynamic roughness laminar wings.

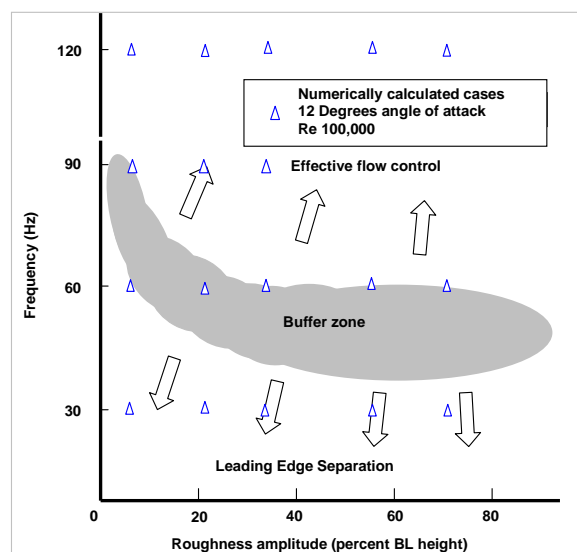
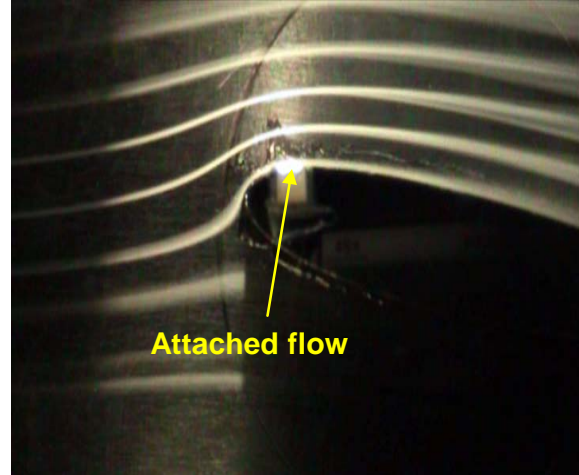


Fig. 7. Effects of amplitude and frequency on flow control at 12 degrees angle of attack and Re of 100,000.

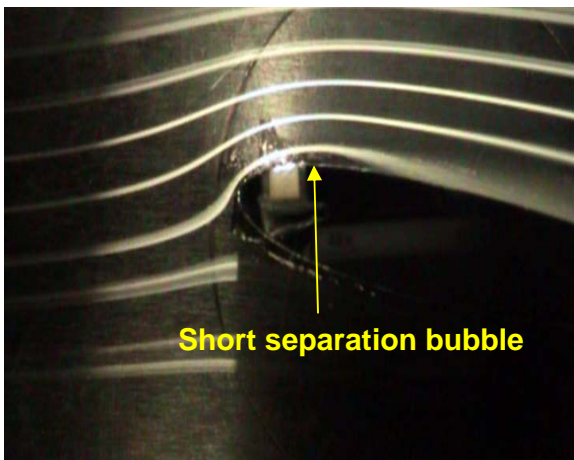
**DYNAMIC ROUGHNESS AS A MEANS OF LEADING EDGE SEPARATION FLOW CONTROL**



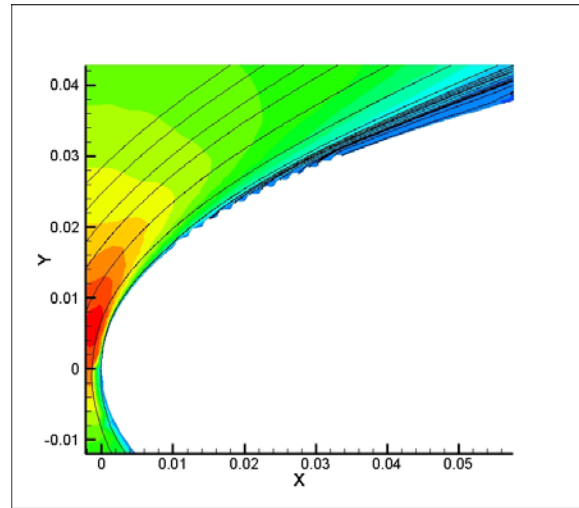
Fig. 8. Dynamic roughness wind tunnel model.



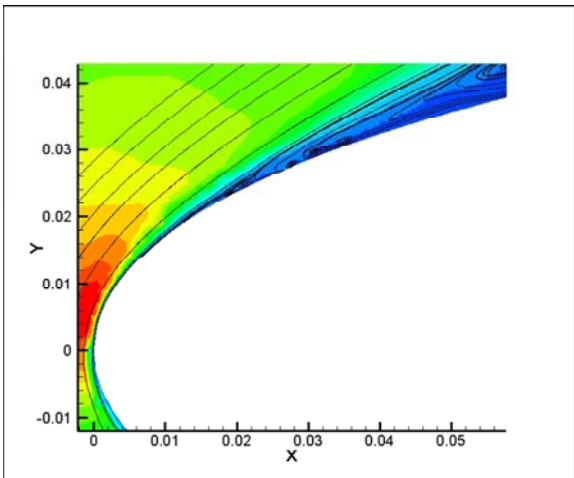
c) Attached flow with dynamic roughness actuated



a) Short separation bubble with dynamic roughness not actuated



d) Numerical prediction of attached flow with dynamic roughness actuated



b) Numerical prediction of short separation bubble with dynamic roughness not actuated

Fig. 9. Numerical and experimental flow physics at 9.5 degrees angle of attack and  $Re$  of 100,000.

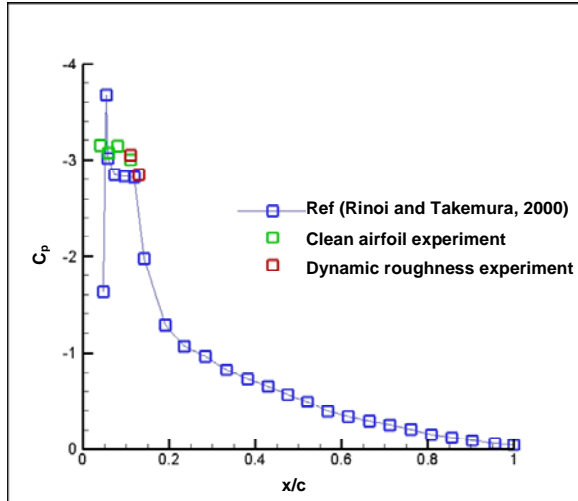
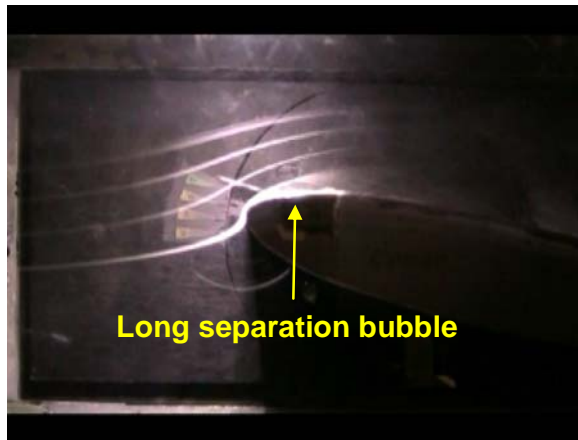
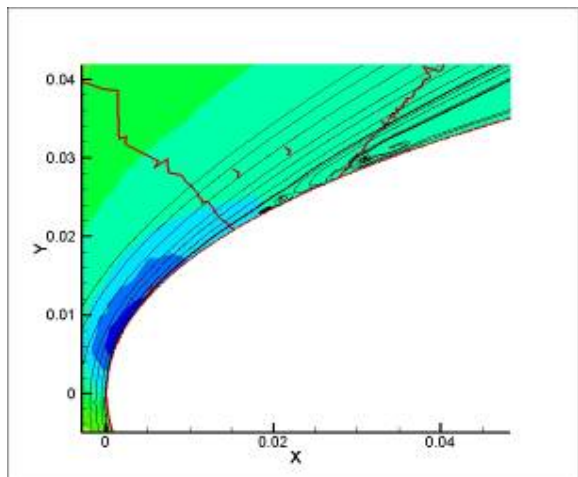


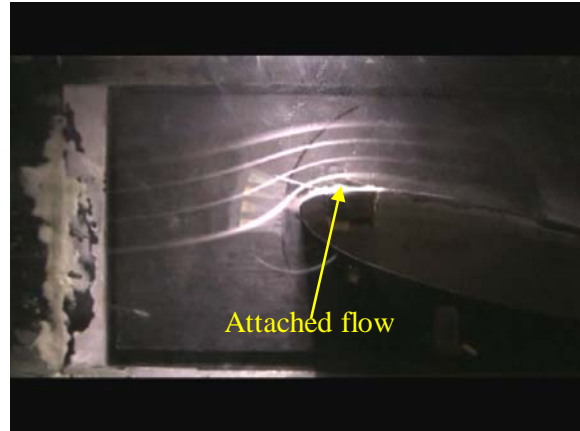
Fig. 10. Experimental pressure distributions at 9.5 degrees angle of attack.



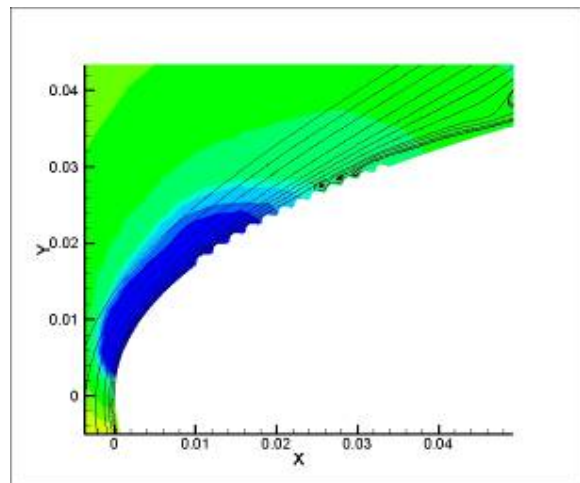
a) Long separation bubble without dynamic roughness actuated



b) Numerical prediction of long separation bubble without dynamic roughness actuated.



c) Attached flow with dynamic roughness actuated



d) Numerical prediction of attached flow with dynamic roughness

Fig. 11. Numerical and experimental flow physics at 12 degrees angle of attack and  $Re$  of 100,000.

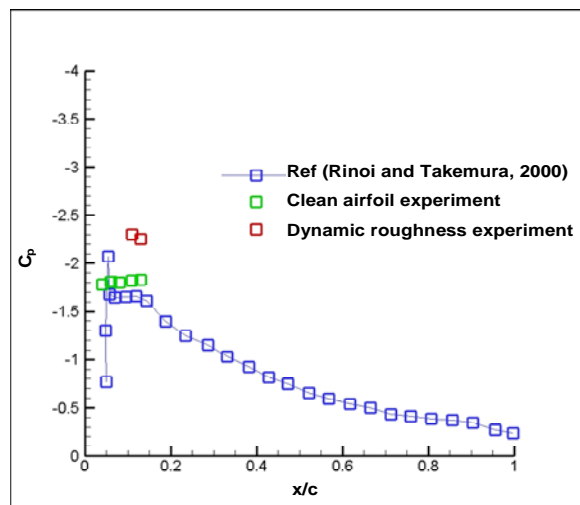


Fig. 12. Experimental pressure distribution at 12 degrees angle of attack